The Journal of Infectious Diseases

MAJOR ARTICLE

Preserved Mucosal-Associated Invariant T Cells in the Cervical Mucosa of HIV-Infected Women with Dominant Expression of the *TRAV1-2–TRAJ20* T Cell Receptor α-Chain

Anna Gibbs,[1,a] Katie Healy,[2,a] Vilde Kaldhusdal,[1] Christopher Sundling,[1] Mathias Franzén-Boger,[1] Gabriella Edfeldt,[1] Marcus Buggert,[3] Julie Lajoie,[4,5] Keith R. Fowke,[4,5,6,7] Joshua Kimani,[4,5,6] Douglas S. Kwon,[8] Sonia Andersson,[9] Johan K. Sandberg,[3] Kristina Broliden,[1] Haleh Davanian,[2] Margaret Sällberg Chen,[2] and Annelie Tjernlund[1]

[1]Department of Medicine Solna, Division of Infectious Diseases, Karolinska Institutet, Department of Infectious Diseases, Karolinska University Hospital, Center for Molecular Medicine, Stockholm, Sweden; [2]Department of Dental Medicine, Division of Oral Diagnostics and Surgery, Karolinska Institutet, Stockholm, Sweden; [3]Department of Medicine Huddinge, Center for Infectious Medicine, Karolinska Institutet, Stockholm, Sweden; [4]Department of Medical Microbiology and Infectious Diseases, University of Manitoba, Winnipeg, Canada; [5]Department of Medical Microbiology, University of Nairobi, Nairobi, Kenya; [6]Partners for Health and Development in Africa, Nairobi, Kenya; [7]Department of Community Health Sciences, University of Manitoba, Winnipeg, Canada; [8]Ragon Institute of MGH, MIT, and Harvard, Massachusetts General Hospital, Cambridge, Massachusetts, USA; and [9]Department of Women's and Children's Health, Division of Obstetrics and Gynecology, Karolinska Institutet, Karolinska University Hospital, Stockholm, Sweden

Background. Mucosa-associated invariant T (MAIT) cells are innate-like T cells with specialized antimicrobial functions. Circulating MAIT cells are depleted in chronic human immunodeficiency virus (HIV) infection, but studies examining this effect in peripheral tissues, such as the female genital tract, are lacking.

Methods. Flow cytometry was used to investigate circulating MAIT cells in a cohort of HIV-seropositive (HIV^+) and HIV-seronegative (HIV^-) female sex workers (FSWs), and HIV^- lower-risk women (LRW). In situ staining and quantitative polymerase chain reaction were performed to explore the phenotype of MAIT cells residing in paired cervicovaginal tissue. The cervicovaginal microbiome was assessed by means of 16S ribosomal RNA gene sequencing.

Results. MAIT cells in the HIV^+ FSW group were low in frequency in the circulation but preserved in the ectocervix. MAIT cell T-cell receptor gene segment usage differed between the HIV^+ and HIV^- FSW groups. The *TRAV1-2–TRAJ20* transcript was the most highly expressed MAIT *TRAJ* gene detected in the ectocervix in the HIV^+ FSW group. MAIT *TRAVJ* usage was not associated with specific genera in the vaginal microbiome.

Conclusions. MAIT cells residing in the ectocervix are numerically preserved irrespective of HIV infection status and displayed dominant expression of *TRAV1-2–TRAJ20*. These findings have implications for understanding the role of cervical MAIT cells in health and disease.

Keywords. HIV; MAIT; cervical mucosa; microbiome; TCR usage; *TRAV1-2–TRAJ20*.

Mucosa-associated invariant T (MAIT) cells are an evolutionary conserved subset of innate-like T cells that express a semi-invariant T-cell receptor (TCR) α chain Vα7.2 (*TRAV1-2–TRAJ33/20/12*) paired with a limited repertoire of TCR β chains, mainly of the *TRBV20* and *TRBV6* gene families [1–5]. MAIT cells are highly abundant in humans, representing up to 10% of T cells in peripheral blood [6]. They are enriched in tissues exposed to the external environment and commensal microbes [7–9]. The main subset of MAIT cells are $CD8^+$, with some being $CD4^-CD8^-$ (double negative [DN]) and a minor subset of $CD4^+$ [10, 11], a distribution mirrored in the female genital tract [12]. TCR-independent MAIT cell responses have recently been shown to control human immunodeficiency virus (HIV) type 1 replication in vitro [13]. Owing to their multifaceted role in host defense, MAIT cells also have immunotherapeutic potential [14, 15].

Studies indicate that MAIT cells are activated in the circulation and in rectal tissue in the acute stage of HIV infection, while chronic infection is associated with a numerical and functional decline in circulating MAIT cells [16–18]. It is presently unknown whether MAIT cells home toward other barrier tissues against the backdrop of HIV-1 infection, such as the

Received 26 January 2022; editorial decision 25 April 2022; accepted 29 April 2022; published online 2 May 2022

[a]A. G. and K. H. contributed equally to this work.

Presented in part: Annual Scientific Review and Planning Meeting, University of Nairobi STD/AIDS Collaborative Centre, Nairobi, Kenya, 28 January 2020.

Correspondence: Annelie Tjernlund, Department of Medicine Solna, Division of Infectious Diseases, Karolinska University Hospital, J7:20, S-171 76 Stockholm, Sweden (annelie.tjernlund@ki.se).

The Journal of Infectious Diseases® 2022;226:1428–40

https://doi.org/10.1093/infdis/jiac171

female genital tract. We have previously shown that MAIT cells reside in the female genital mucosa of HIV-seronegative women and are skewed toward interleukin 17 and interleukin 22 production [12]. MAIT cell tissue repair functions are believed to be modulated by TCR interactions with commensal microbes residing on the mucosal surface [19]. Given that HIV-1 can drive dysbiosis at mucosal barriers [20], it is possible that the virus can shape the cervical MAIT phenotype by indirect mechanisms. In the current study, we aimed to investigate circulating and cervical MAIT cells in chronically HIV$^+$ women and their potential association with the local cervicovaginal microbiome.

METHODS

Ethics Statement

The current study was performed following approval from the ethical review boards representing the Kenyatta National Hospital, the University of Manitoba, and the Regional Ethical Review Board of Stockholm. Written informed consent was obtained from all study participants (Supplementary Data).

Study Populations

HIV-seropositive (HIV$^+$) and HIV-seronegative (HIV$^-$) female sex workers (FSWs) were recruited through the Majengo Sex Worker Clinic in the Pumwani district in Nairobi, Kenya. HIV$^-$ lower-risk women (LRW) (non–sex workers) were recruited through a Maternal Health Clinic at the Pumwani Maternity Hospital. The sample collection was performed during 2009–2016. The detailed characteristics of the study population have been described elsewhere [21–24]. In short, the general inclusion criteria were a minimum age of 18 years, uterus and cervix present, not actively menstruating, antiretroviral treatment naive, no symptomatic or clinically apparent cervical inflammation, and willingness to undergo ectocervical biopsy collection and to abstain from vaginal sex during a healing period of 2 weeks after sampling. All participants were provided with counseling on prevention of sexually transmitted infections, as well as male and female condoms, family planning services, and access to medical care, including HIV treatment, as needed.

Sample Collection

Blood samples were collected by venipuncture using a sodium heparin tube, and peripheral blood mononuclear cells (PBMCs) were separated by Ficoll-Hypaque density gradient centrifugation and cryopreserved. Two ectocervical biopsy specimens (each 3 mm^3) were collected from the superior portion of the ectocervix with a Schubert biopsy forceps (B. Braun Aesculap) and placed in a vial containing RNAlater solution (Qiagen) or immediately snap-frozen and cryopreserved at −80°C and used for in situ staining. For cervicovaginal lavage (CVL) collection, a syringe was used to wash the endocervix with 2 mL of sterile phosphate-buffered saline and to aspirate the lavage from the posterior fornix [25]. The CVL was centrifuged, and the pellet was resuspended in RNAlater (Qiagen) and immediately frozen at −80°C. Detection of HIV-1 RNA in plasma from the blood samples was assessed using real-time reverse-transcription polymerase chain reaction (PCR) [21].

Ectocervical samples were also collected from Swedish volunteers (n = 5), recruited through the Women's Clinic at the Karolinska University Hospital, Stockholm, Sweden [26] (Supplementary Data). Peripheral blood–derived MAIT cells from a healthy blood donor were included. These samples were used to validate the quantitative PCR (qPCR) experiments.

Flow Cytometry

Procedures for flow cytometry staining of PMBCs were adopted from a previous study [27] (Supplementary Data). The antibodies used for flow cytometry analyses are listed in Supplementary Table 1. All manual gating was based on fluorescence-minus-1 gating strategies. The "dump" channel shown in the gating strategy was used to remove dead cells (LIVE/DEAD Aqua Cell Stain$^+$), as well as monocytes/macrophages (CD14$^+$) and B cells (CD19$^+$). MAIT cells were defined as CD45$^+$CD3$^+$CD161^{hi}Vα7.2$^+$.

t-Distributed stochastic neighbor embedding (*t*-SNE) analysis was performed using FlowJo v10.6.1 software. Samples were analyzed using the R-package Cytofkit (version 0.99.0), which includes an integrated pipeline for cytometry data analysis. Clustering was performed using density-based machine learning with ClusterX, and cell subsets were identified by manual inspection of marker expression for each cluster (Supplementary Data).

Quantification of Selected Cytokine Transcripts

The messenger RNA (mRNA) expression of interleukin 7, 18, and 15 (IL-7, IL-18, and IL-15) and ubiquitin C, in ectocervical tissue, was measured by means of qPCR, as described elsewhere [28]. Each sample was run in duplicate, the cycle threshold (Ct) values for each target gene were normalized to ubiquitin C, and the relative abundance of the target genes was calculated by the comparative 2−dCt method [29].

Quantification of MAIT Cell TCR Rearrangements

Peripheral blood–derived MAIT cells from a healthy blood donor were prepared as described elsewhere, by bead sorting using a 5-OP-RU loaded MR1 tetramer and subsequent expansion (National Institutes of Health Tetramer Core Facility, Melbourne, Australia) [30, 31]. Total RNA was extracted using the AllPrep DNA/RNA Micro kit (Qiagen). RNA extraction, from the cryopreserved PBMCs and ectocervical biopsy specimens, followed by complementary DNA synthesis, was performed according to the manufacturer's protocols (Qiagen). Expression of *TRAJ33/20/12*, the TCR constant chain (Cα), as well as glyceraldehyde 3-phosphate dehydrogenase (GAPDH), was performed as described elsewhere [32] (Supplementary

Table 1. Characteristics of Cohort at Time of Sample Collection

Characteristic	Median Value (Range) or No. (%) of Participants			
	HIV^+ FSWs (n = 30)	HIV^- FSWs (n = 31)	HIV^- LRW (n = 23)	*P* Value[a]
Median (range)				
Age, y[b]	40 (24–58)	40 (27–51)	39 (24–49)	NS
Duration of sex work, y[c]	9 (2–26)	10 (4–24)	NA	NS
Time since HIV-1 diagnosis[d]	3 y (9 m-21y)	NA	NA	NA
HIV-1 RNA, copies/mL plasma[e]	6970 (10–648 000)	NA	NA	NA
HIV-1 RNA, copies/mL cervical secretion[f]	20 (20–45 800)	NA	NA	NA
CD4 cell count, cells/mL	554 (121–1737)	NA	NA	NA
Participants, no. (%)				
Bacterial vaginosis[g,h]	7 (23)	7 (25)	3 (14)	NS
Candida[h]	1 (3)	2 (7)	2 (10)	NS
Chlamydia trachomatis[h]	0 (0)	0 (0)	1 (5)	NA
Neisseria gonorrhoeae[h]	0 (0)	0 (0)	0 (0)	NA
Syphilis seropositive[h]	6 (19)	3 (11)	1 (5)	NS

Abbreviations: FSWs, female sex workers; HIV, human immunodeficiency virus; HIV^+, HIV-seropositive; HIV^-, HIV-seronegative; LRW, lower-risk women (non–sex workers); NA, not applicable.NS, nonsignificant.

[a] *P* values based on Mann-Whitney *U* test for continuous and χ^2 test for categorical variables.

[b] Data missing from 2 HIV^- FSWs and 1 HIV^- LRW.

[c] Data missing from 2 HIV^- FSWs.

[d] Data missing from 1 HIV^+ FSWs.

[e] One HIV^+ FSW had plasma viral load below the HIV-1 RNA detection limit of 20 copies/mL and was given the value of 10 copies/mL.

[f] Data missing from 13 HIV^+ FSWs.

[g] Bacterial vaginosis defined by Nugent score.

[h] Data missing from 2 HIV^- FSWs and from 2 HIV^- LRW.

Data, Supplementary Table 2). Each sample was run in duplicate, and the Ct values for each target gene were normalized to Cα or to GAPDH, as indicated in the results section. The relative abundance of the target genes was calculated by the comparative 2^{-dCt} method [29].

In Situ Staining and Image Analysis

In situ staining of the cryopreserved tissue samples to detect MAIT cells was done based on costaining of Vα7.2 and interleukin 18Rα [12, 33] (Supplementary Data). The epithelium and underlying submucosal area, measured from the basal membrane to a depth of approximately 300 μm into the mucosa, were manually outlined in regions of interest with CaseViewer (version 2.3.0) software (3DHistotech). MAIT cells were enumerated by manual counting of $V\alpha7.2^+$interleukin $18R^+$ cells within the region of interest.

16S Ribosomal RNA Cervicovaginal Microbiome Profiling

DNA was extracted from CVL pellets using phenol chloroform. The variable region 4 of the 16S ribosomal RNA gene was sequenced to assess the composition of the cervicovaginal microbiome [34] (Supplementary Data).

Statistical Analysis

The statistical significance of differences between categorical variables was assessed with the χ^2 test and continuous variables with the Mann-Whitney *U* test. Multiple comparison analysis was performed using the Kruskal-Wallis test, followed by the Dunn post hoc test. The Spearman rank correlation coefficient test was used to assess correlations. All tests were 2 sided, and differences were considered significant at $P < .05$. All statistical analyses were performed using Prism 9.1.2 software (GraphPad) (Supplementary Data).

RESULTS

Clinical Characteristics of Study Cohort

The Kenyan study cohort was divided into 3 groups: HIV-seropositive (HIV^+) female sex workers (FSWs; n = 30), HIV-seronegative (HIV^-) FSWs (n = 31), and HIV^- LRW (n = 23). The first group was the experimental group, and the other 2 groups served as controls; the HIV^- FSWs provided a control for the influence of vaginal douching practices and the impact of sex work (Table 1).

All study participants were within the same age range. The prevalence of bacterial vaginosis and sporadic sexually transmitted infections were similar across the groups. The HIV^+ and HIV^- FSWs had similar durations of sex work (median, 9 years) and time since HIV diagnosis (median, 3 years). The HIV^+ FSWs had no history of AIDS-defining illnesses.

Low Frequency of Circulating MAIT Cells in HIV^+ Women

PBMCs were assessed with flow cytometry to enumerate and characterize the phenotype of circulating MAIT cells

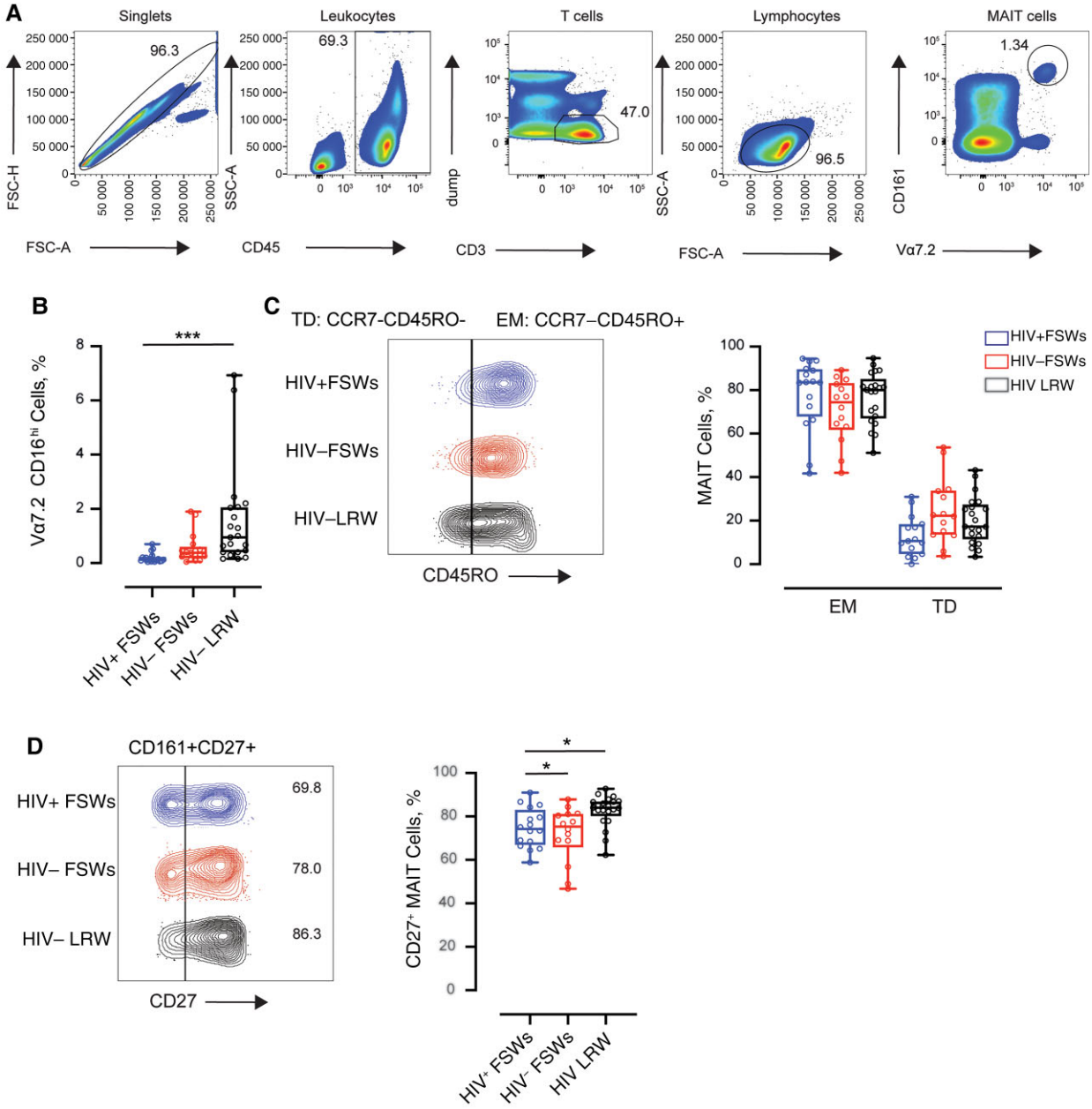

Figure 1. Enumeration and memory phenotype of blood-derived mucosa-associated invariant T (MAIT) cells. *A,* Representative figures illustrating flow cytometry identification of Vα7.2^{+}CD161^{hi} MAIT cells. Abbreviations: FSC-A, forward scatter area; FSC-H, forward scatter height; SSC-A, side scatter area. *B,* Box plots showing the percentage of Va7.2^{+}CD161^{hi} MAIT cells among total CD3^{+} T cells from peripheral blood mononuclear cell (PBMC) samples obtained from human immunodeficiency virus (HIV)–seropositive (HIV^{+}) female sex workers (FSWs) (n = 18), HIV-seronegative (HIV^{-}) FSWs (n = 17), and HIV^{-} lower-risk women (LRW) (n = 21). *C,* Representative samples of blood-derived MAIT cells expressing CCR7 and CD45RO, which were used to define different memory phenotypes in the HIV^{+} FSWs (n = 15), HIV^{-} FSWs (n = 14), and HIV^{-} LRW (n = 21) groups. Box plots show the percentage of MAIT cells expressing an effector memory (EM; CCR7^{-}CD45RO^{+}) or terminally differentiated (TD; CCR7^{-}CD45RO^{-}) phenotype in the 3 study groups. *D,* Representative sample of blood-derived MAIT cells expressing CD27 and box plots showing the percentage of CD27^{+} MAIT cells among total MAIT cells in the 3 study groups: HIV^{+} FSWs (n = 16; *blue*), HIV^{-} FSWs (n = 14; *red*), and HIV^{-} LRW (n = 21; *black*). Box plots represent medians, with interquartile range and range, and each data point represents a single participant. Statistical significance was determined using the Kruskal-Wallis test, followed by the Dunn post hoc test; *P* values in the figure are based on Dunn post hoc tests. **P* < .05; ****P* < .001. This figure is available in black and white in print and in color online.

(CD45^{+}CD3^{+}CD161^{hi}Vα7.2^{+}) (Figure 1A). The percentage of blood MAIT cells was significantly lower in HIV^{+} FSWs than in HIV^{-} LRW (Figure 1B). In all study groups, the majority of MAIT cells expressed a CCR7^{-}CD45RO^{+} effector memory phenotype, with the remaining MAIT cells expressing a terminally differentiated CCR7^{-}CD45RO^{-} phenotype. No significant differences were seen between the groups for the effector memory and terminally differentiated phenotypes (Figure 1C).

The expression of the costimulatory molecule CD27, which can be used together with other T-cell markers for memory differentiation [35], was significantly lower in the HIV$^+$ FSW group (Figure 1D).

Activated Phenotype in Circulating MAIT Cells Among HIV$^+$ Women

Next, an unbiased analysis of the expression of activation markers (CD69, CD38, HLA-DR, and programmed cell death 1 protein [PD-1]) in circulating MAIT cells was performed using *t*-SNE dimensionality reduction and cluster analysis (Figure 2A–2C). Among the 11 MAIT cell clusters, the size of clusters 4, 6, and 7 was significantly altered in the HIV$^+$ FSW group (Figure 2A).

Cells in cluster 4 consisted of activated MAIT cells (CD38$^+$PD-1$^+$CD8$^+$) of a terminal effector (CD45RO$^-$CD27$^+$) profile, and a significantly lower percentage of HIV$^+$ FSWs expressed this phenotype compared with the HIV$^-$ LRW group. Cells in cluster 6 comprised activated (CD38$^+$HLA-DR$^+$PD-1$^+$) DN MAIT cells with a transitional memory phenotype (CD45RO$^+$CD27$^+$). The HIV$^+$ FSWs had a significantly higher percentage of this phenotype than the HIV$^-$ FSWs (Figure 2A–2C). Cells in cluster 7 were nonactivated (CD38$^-$HLA-DR$^-$PD-1$^-$) DN MAIT cells with a terminally differentiated (CD45RO$^-$CD27$^-$) phenotype. The HIV$^+$ FSWs had a significantly lower percentage of this cell population compared with the HIV$^-$ FSWs, but not compared with the HIV$^-$ LRW group (Figure 2A–2C). Collectively, 2 main clusters were seen, one representing activated MAIT cells (clusters 1, 2, 4, 6, 9, and 10) and the other nonactivated MAIT cells (clusters 3, 5, 7, 8, and 11) (Figure 2C). All 3 study groups were dominated by the activated phenotype cluster, compared with the nonactivated cluster. No significant difference was seen between the 3 study groups with regard to the percentage of activated or nonactivated MAIT cells (Figure 2D).

Flow cytometric analysis of activation markers on MAIT cells revealed that these cells from the HIV$^+$ FSW group, compared with the HIV$^-$ FSW and HIV$^-$ LRW groups, expressed significantly higher levels of CD38 and HLA-DR (both $P <$ .001) but not the early activation marker CD69 or the inhibitory receptor PD-1 (Figure 3A). Moreover, the percentage of circulating MAIT cells was inversely correlated with highly activated MAIT cells ($\rho = -0.49$; $P = .003$) (Figure 3B).

In the HIV$^+$ FSWs, the percentage of PD-1$^+$ MAIT cells was positively correlated with the HIV-1 plasma viral load (in HIV-1 RNA copies per milliliter of plasma) ($r = 0.56$; $P = .03$), and significant negative correlations were seen between the percentage of PD-1$^+$ and HLA-DR$^+$ MAIT cells and the CD4/CD8 ratio ($r = -0.51$; $P = .05$) (Supplementary Figure 1).

Abundance of DN MAIT cells may be due to downregulation of the CD8 coreceptor and associated with activation and exhaustion of MAIT cells [11]. The HIV$^+$ FSWs had fewer CD8$^+$ MAIT cells than the HIV$^-$ LRW group (Figure 3C). The HIV$^+$ FSWs had a lower percentage of CD8$^+$ MAIT cells than DN MAIT cells, which was not observed in the HIV$^-$ FSW and HIV$^-$ LRW groups. The CD4$^+$ MAIT cells were the smallest subset in all 3 study groups. A positive correlation was seen between the percentage of DN MAIT cells and HIV plasma viral load ($r = 0.55$; $P = .03$) (Figure 3D).

MAIT Cells in the Ectocervix of HIV$^+$ and HIV$^-$ Women

In situ staining was performed to quantitatively assess the MAIT cells in ectocervical tissue samples. MAIT cells were located close to the basal membrane (Figure 4A). Owing to limited sample availability, MAIT cells were quantified only in the HIV$^+$ FSW and HIV$^-$ LRW groups. The average tissue area analyzed was comparable between the HIV$^+$ FSW and HIV$^-$ LRW groups (median, 2.2 vs 2.7 mm^2, respectively). No significant difference was seen in the number of Vα7.2$^+$IL-18R$^+$ cells per square millimeter in the ectocervix of the HIV$^+$ FSW ($n = 7$) and HIV$^-$ LRW ($n = 8$) groups (Figure 4B). However, owing to the small sample size, this finding should be interpreted cautiously.

We next assessed the relative mRNA expression of IL-18, IL-15, and IL-7 in the ectocervical biopsy specimens. The HIV$^+$ FSWs displayed significantly lower levels of IL-18 and IL-7 than the HIV$^-$ LRW but not the HIV$^-$ FSWs ($P = .005$ and $P = .01$, respectively). The IL-15 expression was comparable between the groups (Figure 4C). Decreased levels of cervical cytokines could potentially affect the functionality of MAIT cells at this site.

High Expression of *TRAJ20* in Blood and Ectocervix of Kenyan Women but No Association Between Sites

To assess whether the MAIT TCR expression differs between circulating and ectocervical residing MAIT cells, the expression of the transcripts *TRAV1-2–TRAJ33*, *TRAV1-2–TRAJ20,* and *TRAV1-2–TRAJ12* (hereafter referred to as *TRAJ33*, *TRAJ20*, and *TRAJ12*, respectively) was measured using reverse-transcription qPCR (Supplementary Data). The expression of *TRAJ33*, *TRAJ20*, and *TRAJ12* was normalized to the TCR constant chain (Cα) gene expression to control for numerical differences in T cells between the study groups. In contrast with findings of previous studies, *TRAJ20* was the dominant *TRAJ* seen in the majority of both the PBMCs and the ectocervical samples in the Kenyan cohort. No significant difference in the proportion of the *TRAJ* expression was seen in the PBMC samples. In the ectocervical compartment, the HIV$^+$ FSWs had significantly more *TRAJ20* than *TRAJ33* and *TRAJ12* ($P <$ .001), while the HIV$^-$ FSWs and HIV$^-$ LRW had significantly more *TRAJ20* than *TRAJ12* ($P = .004$) and significantly more *TRAJ33* than *TRAJ12* ($P = .001$) (Figure 5A). Paired analysis of TCR gene expression in all 3 study groups combined did

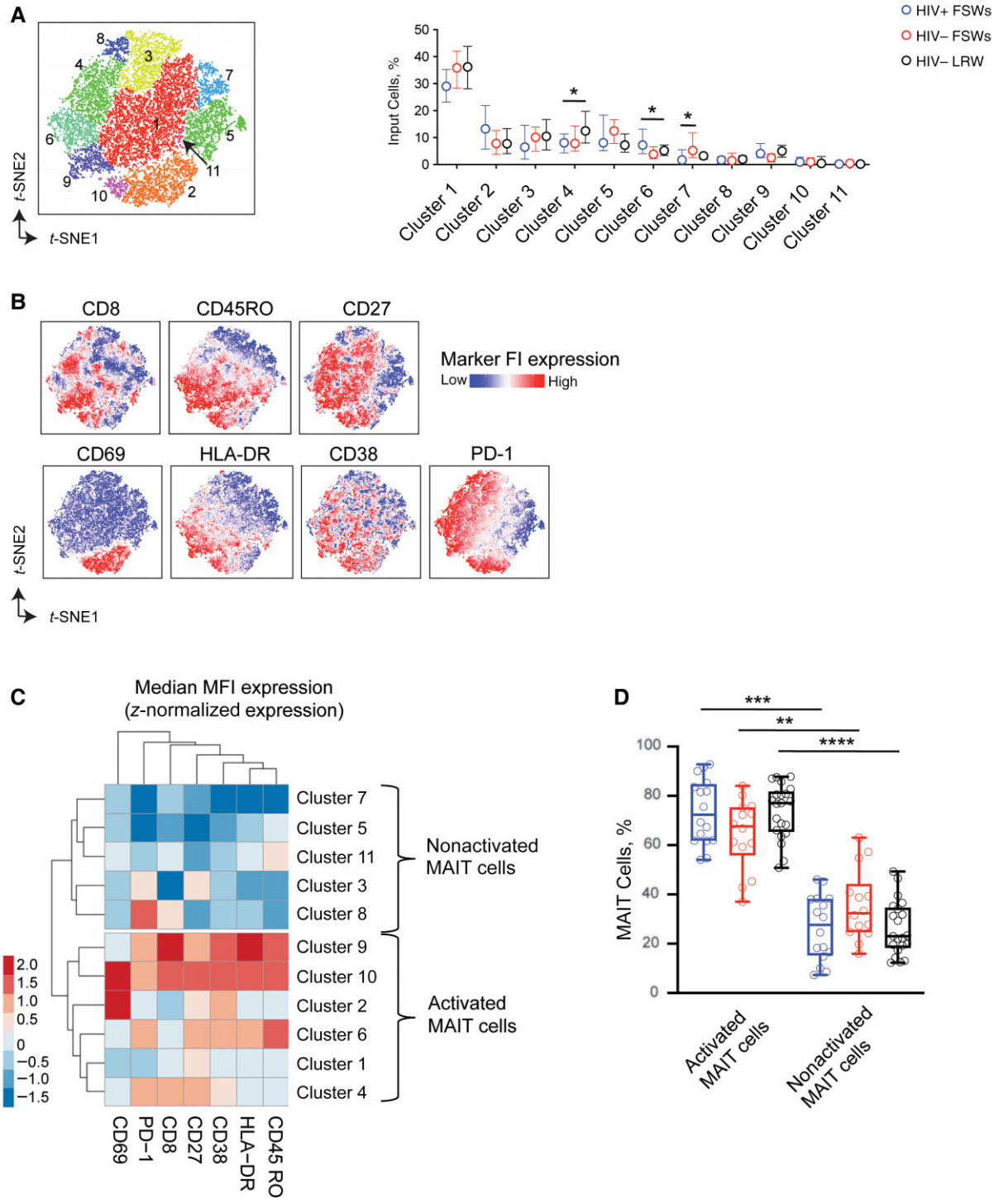

Figure 2. *t*-Distributed stochastic neighbor embedding (*t*-SNE) analysis followed by clustering of flow cytometry peripheral blood mononuclear cell (PBMC) data. *B, t*-SNE plots showing the fluorescent intensity (FI) expression of CD8, CD45RO, CD27, CD69, HLA-DR, CD38, and programmed cell death 1 protein (PD-1) for analyzed MAIT cells. *C,* Heat map showing median fluorescent intensity (MFI) expression of individual markers within each cluster, with MFI expression levels normalized to columns. *D,* Box plots showing the percentages of activated and nonactivated MAIT cells in the 3 study groups: human immunodeficiency virus (HIV)–seropositive (HIV^+) female sex workers (FSWs) (n = 16; *blue*), HIV-seronegative (HIV^-) FSWs (n = 14; *red*), and HIV^- lower-risk women (LRW) (n = 21; *black*). Box plots represent medians with interquartile range and range, and each data point represents a single participant. Statistical significance was determined using the Wilcoxon test for paired analyses and the Kruskal-Wallis test followed by Dunn post hoc test for unpaired analyses; *P* values in the figure are based on Dunn post hoc tests. $^*P < .05$; $^{**}P < .01$; $^{****}P < .0001$. This figure is available in black and white in print and in color online.

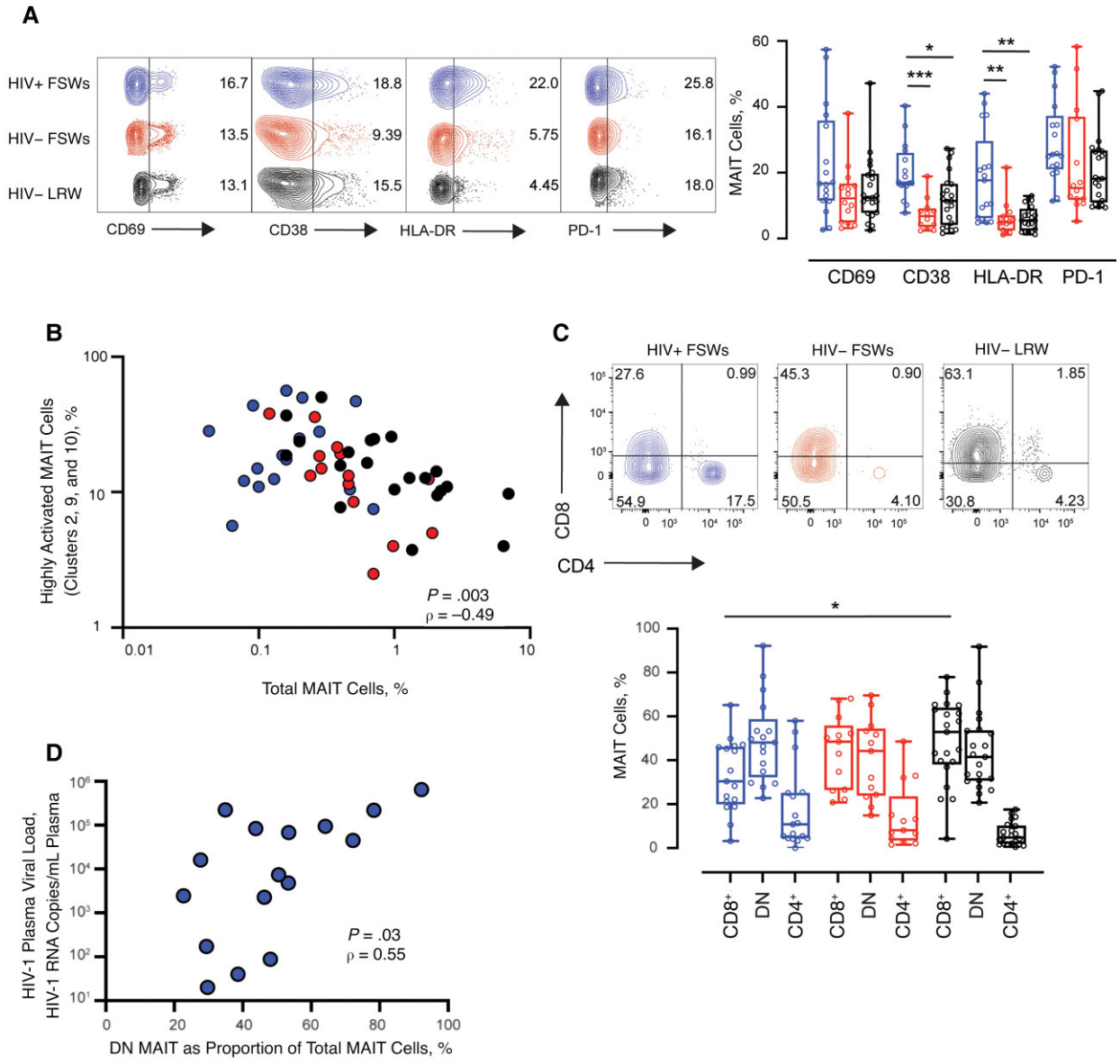

Figure 3. Activation status of blood-derived mucosa-associated invariant T (MAIT) cells. *A,* Representative images and box plots showing the percentages of $CD69^+$, $CD38^+$, $HLA\text{-}DR^+$, and programmed cell death 1 protein $(PD\text{-}1)^+$ MAIT cells in the total MAIT cell pool among human immunodeficiency virus (HIV)–seropositive (HIV^+) female sex workers (FSWs) (n = 17), HIV-seronegative (HIV^-) FSWs (n = 13), and HIV^- lower-risk women (LRW) (n = 21). CD38 data were missing from 1 HIV^+ FSW and 2 HIV^- FSWs. *B,* The percentage of circulating MAIT cells from all participants in the 3 study groups was correlated with highly activated MAIT cells (present in clusters 2, 9 and 10 that are visualized in Figure 2C). *C,* Representative image and box plots from the 3 study groups illustrating identification of $CD8^+$, $CD4^+$ or double-negative (DN) blood MAIT cells. *D,* Correlation between the percentage of DN MAIT cells among total MAIT cells in peripheral blood mononuclear cell (PBMC) samples and the HIV-1 plasma viral load (n = 16). HIV^+ FSWs are depicted in blue, HIV^- FSWs in red, and HIV^- LRW in black. Box plots represent medians, with interquartile range and range, and each data point represents a single participant. Statistical significance was determined using the Kruskal-Wallis test, followed by Dunn post hoc test; *P* values in the figure are based on Dunn post hoc tests. The Spearman rank correlation coefficient test was used to assess correlations. $*P < .05$; $**P < .01$; $***P < .001$. This figure is available in black and white in print and in color online.

not reveal any significant differences between PBMCs and ectocervical samples (Figure 5B).

Next, we investigated whether HIV-1 infection status affected the distribution of the TCR usage by comparing the normalized *TRAJ33/20/12* gene segment expression between the study groups. In the PBMC samples, no significant differences in expression of the TCR *TRAV1-2* joining genes were seen between the 3 study groups. In the ectocervical samples, HIV^+ FSWs had significantly higher relative expression of *TRAJ20* than HIV^-LRW and significantly higher relative expression of *TRAJ12* than both HIV^- FSWs and HIV^- LRW ($P = .002$) (Figure 5C). Similar patterns were seen when the qPCR data were normalized to GAPDH instead of TCR Cα (Supplementary Figure 2).

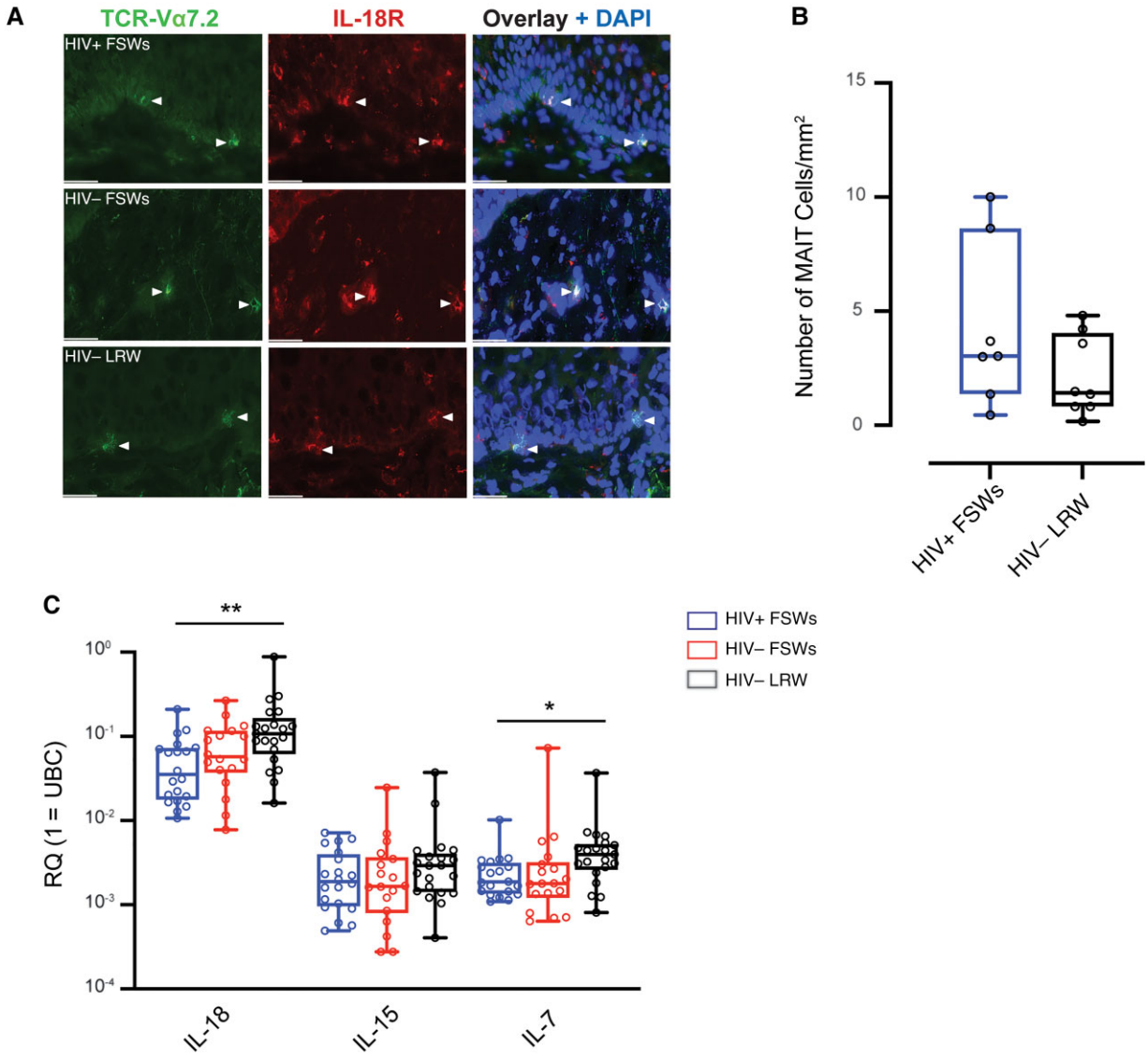

Figure 4. Assessment of mucosa-associated invariant T (MAIT) cells and cytokines in the ectocervical mucosa. *A,* Representative immunofluorescence images of ectocervical tissue sections from human immunodeficiency virus (HIV)–seropositive (HIV^+) female sex workers (FSWs) (*first row*), HIV-seronegative (HIV^-) FSWs (*second row*), and HIV^- lower-risk women (LRW) (*third row*), sections stained for Vα7.2 (*green*), interleukin 18Rα (IL-18Rα) (*red*) and 4′,6-diamidino-2-phenylindole (DAPI) (*blue*). DAPI was used as a counterstain for visualization of cell nuclei. The double positive cells (*third column*) are indicated by white arrows. Images were obtained with ×20 objectives; scale bars represent 25 μm. Abbreviation: TCR, T-cell receptor. *B,* Box plot showing the number of $V\alpha7.2^+IL\text{-}18R\alpha^+$ cells per square-millimeter tissue area in HIV^+ FSWs (n = 7; *blue*) and HIV^- LRW (n = 8; *black*). *C,* Box plots showing the relative messenger RNA expression of interleukin 18, 15, and 7 (IL-18, IL-15, and IL-7) normalized to ubiquitin C (UBC) in ectocervical tissue samples from HIV^+ FSWs (n = 20; *blue*), HIV^- FSWs (n = 18; *red*), and HIV^- LRW (n = 21; *black*). Abbreviation, RQ, relative quantification. Box plots represent medians, with interquartile range and range, and each data point represents a single participant. Statistical significance was determined using the Kruskal-Wallis test, followed by Dunn post hoc test; *P* values in the figures are based on Dunn post hoc tests. $*P < .05$; $**P < .01$. This figure is available in black and white in print and in color online.

The sum of the percentage of each of the 3 *TRAV1-2–TRAJ* rearrangements of the TCR Cα was calculated to estimate the total levels of MAIT cells. The HIV^+ FSWs had the lowest percentage of MAIT TCR α chain expression in the PBMC samples, while the HIV^- LRW had the highest percentage. Interestingly, an inverse effect was observed in the ectocervical samples (Figure 5D). No correlation was seen between the cervical HIV RNA levels and levels of circulating or cervical MAIT cells (Supplementary Data).

Assessment of the Vaginal Bacterial Microbiome and MAIT Cell *TRAJ* Expression in Ectocervical Tissue

The cervicovaginal microbiome composition was assessed with 16S ribosomal RNA gene sequencing of CVL samples from the

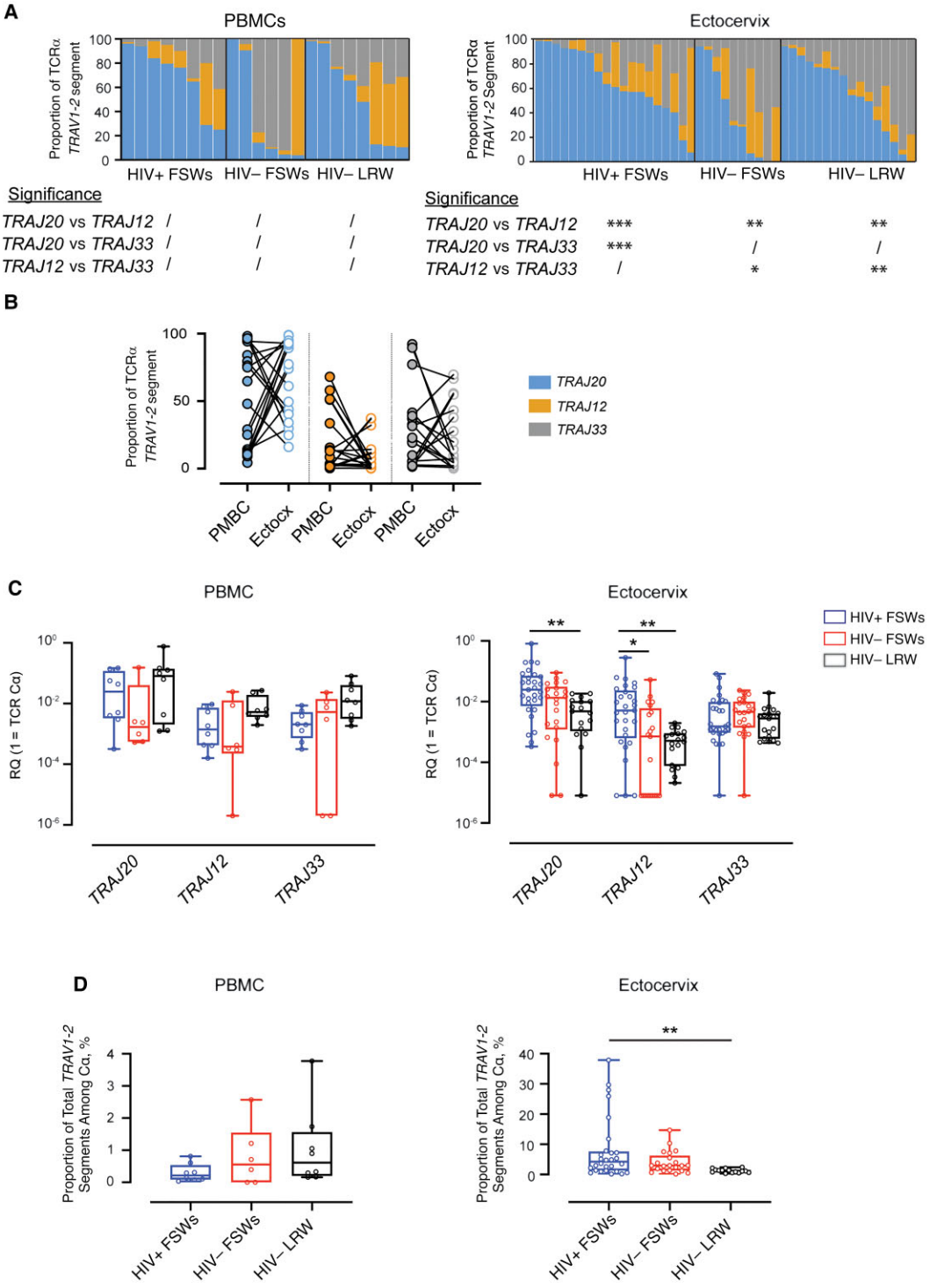

Figure 5. Relative gene expression of mucosa-associated invariant T (MAIT)–specific T-cell receptor (TCR) segments in peripheral blood mononuclear cells (PBMCs) and ectocervical tissue samples. *A,* Stacked bars showing the proportion of the relative gene transcript of *TRAJ20/33/12* normalized to the TCR constant α chain (Cα) in PBMC (*left*) and ectocervical (*right*) samples from human immunodeficiency virus (HIV)–seropositive (HIV^+) female sex workers (FSWs) (n = 8 for PBMCs and n = 29 for ectocervical samples), HIV-seronegative (HIV^-) FSWs (n = 6 and n = 22, respectively), and HIV^- lower-risk women (LRW) (n = 8 and n = 19). *B,* Graph comparing the proportions of *TRAJ20*, *TRAJ33,* and *TRAJ12* expression in paired PBMC and ectocervical samples from HIV^+ FSWs (n = 8), HIV^- FSWs (n = 3), and HIV^- LRW (n = 7). *C,* Box plots showing the relative quantification (RQ: 1 = Ca) of the MAIT-specific TCR segments *TRAJ20*, *TRAJ33,* and *TRAJ12* in PBMC and ectocervical samples from HIV^+ FSWs (n = 8 for PBMCs and n = 29 for ectocervical samples), HIV^- FSWs (n = 6 and n = 22, respectively), and HIV^- LRW (n = 8 and n = 19). *D,* Percentage of total *TRAV1-2* gene segments in PBMC (*left*) and ectocervical (*right*) samples from HIV^+ FSWs (n = 8 for PBMCs and n = 29 for ectocervical samples; *blue*), HIV^- FSWs (n = 6 and n = 22; *red*), and HIV^- LRW (n = 8 and n = 19; *black*). Samples with cycle threshold (Ct) values of ≤40 were given a Ct value 2 log lower than lowest detected levels. Box plots represent medians, with interquartile range and range, and each data point represents a single participant. Statistical significance was determined using the Kruskal-Wallis test, followed by the Dunn post hoc test; *P* values in the figure are based on Dunn post hoc tests. $*P < .05$; $**P < .01$; $***P < .001$. This figure is available in black and white in print and in color online.

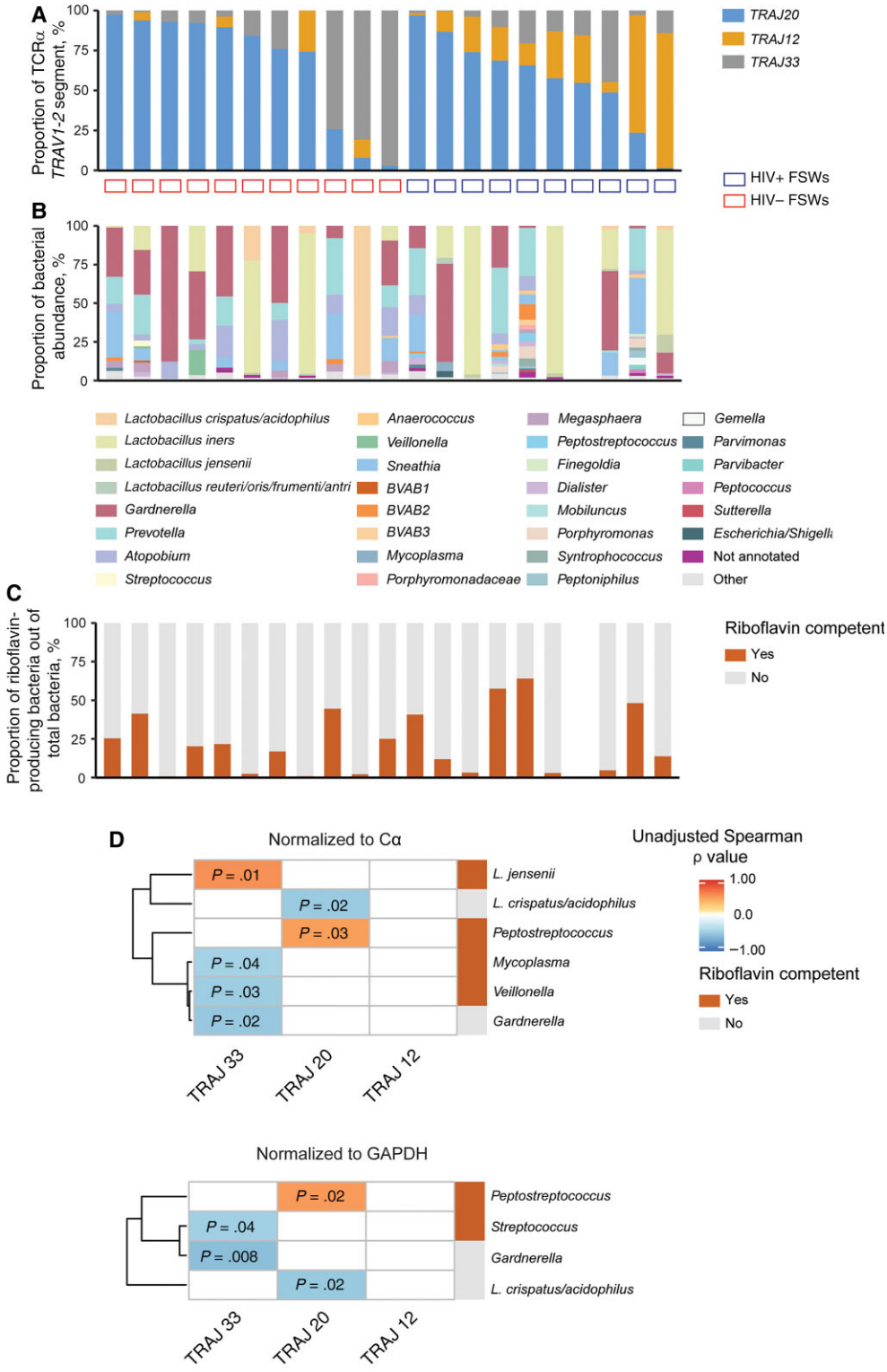

Figure 6. Cervicovaginal microbial composition. *A,* Stacked bar plot showing relative abundance of the 3 *TRAV1-2* joining gene segments in ectocervical samples from human immunodeficiency virus (HIV)–seropositive (HIV^+) (n = 10) and HIV-seronegative (HIV^-) (n = 11) female sex workers (FSWs). *B,* Stacked bar plot showing relative abundance of the cervicovaginal microbial composition (all bacteria genera that had a proportion of <1% per sample were merged into the group labeled "Other"). *C,* Proportion of PICRUSt2 (version 2.3.0) software–predicted riboflavin-producing bacteria in the cervicovaginal lavage samples from HIV^+ (n = 9) and HIV^- (n = 11) FSWs. Samples are ordered according to decreasing *TRAJ20* proportions in the 2 study groups. *D,* Pairwise Spearman ρ correlations were performed between total sum scaling (TSS)-normalized vaginal microbiome abundance (at genus level + *Lactobacillus* spp.), and the relative gene expression of *TRAJ20, TRAJ12,* or *TRAJ33* segments normalized to the T-cell receptor (TCR) constant α chain (Cα) (*upper heat map*) and to glyceraldehyde 3-phosphate dehydrogenase (GAPDH) (*lower heat map*) in ectocervical tissue samples from HIV^+ (n = 9) and HIV^- (n = 11) FSWs. Unadjusted Spearman ρ values and and unadjusted *P* values are shown in the heat maps. This figure is available in black and white in print and in color online.

HIV^+ and HIV^- FSW groups (Supplementary Data). No significant differences were seen in either the proportion of the ectocervical MAIT TCR gene segment expression or the cervicovaginal microbiome composition between the 2 study groups (Figure 6A–6C and Supplementary Tables 3–5).

Both the HIV^+ and HIV^- FSW groups displayed a diverse cervicovaginal microbiome. No significant correlation was seen, after adjustment for multiple comparisons (false discovery rate, <0.05), between the total sum scaling (TSS)-normalized microbiome abundance, and the relative gene expression of *TRAJ33, TRAJ20,* and *TRAJ12* segments (Figure 6D and Supplementary Data).

DISCUSSION

The current study shows that while MAIT cells are reduced in the circulation of HIV^+ women, they are numerically preserved in the ectocervical mucosa. High levels of *TRAJ20* usage were seen in MAIT cells in both blood and ectocervical tissue, and this was particularly dominant in the ectocervical compartment of the HIV^+ women.

Severe depletion of circulating MAIT cells, with functional impairment of those that remain, is a hallmark of untreated chronic HIV-1 infection [16, 17], a phenotype we also observed in this cohort of HIV^+ FSWs. The majority of circulating MAIT cells, regardless of HIV status, displayed activated phenotypes, which is different from the patterns observed in healthy Swedish volunteers [17]. In addition to numerical decline, we found that remaining circulating MAIT cells displayed an effector memory phenotype and up-regulated activation markers, predominantly CD38 and HLA-DR. During acute HIV infection, MAIT cells acquire an activated phenotype at the peak of the HIV viremia, followed by decreased activation and numerical loss that is also inversely correlated with increased PD-1 expression and functional exhaustion [18]. Here, we observed that the frequencies of activated MAIT cells and PD-1^+ MAIT cells were inversely correlated with the total frequency of MAIT cells in blood. Furthermore, PD-1^+ MAIT cells were correlated to clinical parameters representing progressive HIV infection, suggesting a gradual exhaustion of the MAIT cell compartment over the course of infection.

The majority of MAIT cells are $CD8^+$, with smaller subsets of DN and $CD4^+$ cells [36]. Early in HIV infection, MAIT cells undergo a subset redistribution involving CD8 down-regulation and subsequent expansion of the DN pool, which is likely due to increased cellular activation [11, 18]. In line with this, we showed a higher frequency of DN than than of $CD8^+$ MAIT cells in HIV^+ women. The frequency of DN MAIT cells was correlated with HIV plasma viral load, confirming that virus replication has a role in skewing the subset profile of MAIT cells. Because DN MAIT cells are more prone to apoptosis than $CD8^+$ MAIT cells [11], this effect may contribute to the diminished pool of circulating MAIT cells in HIV^+ women.

It has been suggested that the numerical decline of circulating MAIT cells in HIV infection is due to their migration to the mucosal tissues, key sites of inflammation, viral replication, and microbial translocation [37]. Here, we observed that MAIT cells were also preserved in the cervical epithelium and underlying connective tissue, in agreement with our group's previous study [12]. Similar frequencies of MAIT cells were seen in the HIV^+ FSWs and the HIV^- LRW, indicating that this preservation is independent of HIV infection status. An overall limitation of the study is limited tissue availability; thus, MAIT cell frequency was assessed in only a few individuals, and functional studies of cervical MAIT cells could not be performed.

The Kenyan study participants demonstrated diverse TCR usage among their blood-derived MAIT cells, with prominent *TRAJ20* composition. Moreover, the *TRAJ20* rearrangement was also the most commonly detected in the ectocervix, regardless of HIV status. However, the HIV^+ women displayed the highest levels of *TRAJ20.* The qPCR data revealed that the HIV^+ women had higher levels of MAIT cells in their cervical mucosa than the control groups, in contrast with what was seen in the circulation. We have previously shown that HIV^+ women from the Kenyan cohort had high mRNA levels of inflammatory cytokines in their cervical compartment [21], and this inflammation could promote increased homing of the MAIT cells to this environment. In the current study, no correlation was seen between HIV cervical shedding and the percentage of circulating MAIT cells or between HIV cervical shedding and cervical *TRAJ33/20/12* gene segment expression. Moreover, no significant difference in TCR gene usage was noted between circulating and cervical-residing MAIT cells. A possible explanation for this is the highly vascularized anatomy of the female genital tract, resulting in a closer similarity with MAIT cells in the blood than found in other mucosal tissues [38, 39].

Local microbiota play a pivotal role in the early development of MAIT cells in the thymus and later expansion in peripheral tissues [8, 40]. Previous studies have shown that gut dysbiosis in HIV^+ individuals is associated with less functional MAIT cells [41]. The Kenyan women in our study had a diverse microflora, with low abundance of *Lactobacillus* and high abundance of *Gardnerella* and *Prevotella* genera. No significant correlations were seen between the cervicovaginal microbiota and MAIT TCR gene expression. It is worth noting that this analysis was performed only on the mRNA level and may not accurately depict TCR expression on the cell surface. Thus, the composition of MAIT cell TCR usage in the cervical compartment needs to be further assessed, including the TCR β chain that displays a broader repertoire [42].

In summary, MAIT cells are depleted in blood but preserved in the cervical mucosa during HIV-1 infection, potentially

indicating the importance of their preservation at barrier tissue. A distinct dominance of *TRAJ20* in the ectocervical compartment during HIV-1 infection opens up the possibility of microbe-specific repertoire shaping.

Supplementary Data

Supplementary materials are available at *The Journal of Infectious Diseases* online (http://jid.oxfordjournals.org/). Supplementary materials consist of data provided by the author that are published to benefit the reader. The posted materials are not copyedited. The contents of all supplementary data are the sole responsibility of the authors. Questions or messages regarding errors should be addressed to the author.

Notes

Acknowledgments. We thank the study participants and the staff at the Partners for Health and Development in Africa, Nairobi, Kenya, especially the staff of the Majengo/Pumwani clinics. We specifically thank Taha Hirbod, Rupert Kaul, Terry B. Ball, Kenneth Omollo, and Geneviève Boily-Larouche for the establishment of the clinical infrastructure for tissue sampling at the University of Nairobi Institute for Tropical and Infectious Diseases. We are grateful for the technical assistance provided by Fariba Foroogh and Jiawu Xu. The MR1 tetramer was developed by James McCluskey, Jamie Rossjohn, and David Fairlie, produced by the National Institutes of Health Tetramer Core Facility, and kindly distributed by the University of Melbourne.

Financial support. This research was supported by the Tore Nilsons Research Foundation for Medical Research (grant 2019-00757 to A. G.), Karolinska Institutet Research Foundation (grant 2020-02053 to A. G.), the Swedish Society of Medicine (grant SLS 775201 to A. G.), the Swedish Physicians Against AIDS Research Foundation (grant FOa2018-0008 to A. G.), the Swedish Research Council (grant VR-MH-2019-01754 to K. B.), the Swedish National Research Foundation (grant 2020-02924 to M. S. C.), the Swedish Cancer Society (grant 19 0495 Pj 01H to M. S. C.), the Karolinska Institutets KID PhD training program (grants OF11211252 to K. H. and M. S. C. and 2-6787/2018 to M. F. B. and A. T.), and Olle Engkvists Stiftelse (grant 188-0156 to A. T.) Funding to pay the Open Access publication charges for this article was provided by BIBSAM.

Potential conflicts of interest. All authors: No reported conflicts. All authors have submitted the ICMJE Form for Disclosure of Potential Conflicts of Interest.

References

1. Fergusson JR, Smith KE, Fleming VM, et al. CD161 defines a transcriptional and functional phenotype across distinct human T cell lineages. Cell Rep **2014**; 9:1075–88.
2. Reantragoon R, Kjer-Nielsen L, Patel O, et al. Structural insight into MR1-mediated recognition of the mucosal associated invariant T cell receptor. J Exp Med **2012**; 209: 761–74.
3. Tilloy F, Treiner E, Park SH, et al. An invariant T cell receptor α chain defines a novel TAP-independent major histocompatibility complex class Ib-restricted α/βT cell subpopulation in mammals. J Exp Med **1999**; 189:1907–21.
4. Corbett AJ, Eckle SBG, Birkinshaw RW, et al. T-cell activation by transitory neo-antigens derived from distinct microbial pathways. Nature **2014**; 509:361–5.
5. Le Bourhis L, Martin E, Péguillet I, et al. Antimicrobial activity of mucosal-associated invariant T cells. Nat Immunol **2010**; 11:701–8.
6. Gherardin NA, Loh L, Admojo L, et al. Enumeration, functional responses and cytotoxic capacity of MAIT cells in newly diagnosed and relapsed multiple myeloma. Sci Rep **2018**; 8:4159.
7. Provine NM, Klenerman P. MAIT cells in health and disease. Annu Rev Immunol **2020**; 38:203–28.
8. Treiner E, Duban L, Bahram S, et al. Selection of evolutionarily conserved mucosal-associated invariant T cells by MR1. Nature **2003**; 422:164–9.
9. Sobkowiak MJ, Davanian H, Heymann R, et al. Tissue-resident MAIT cell populations in human oral mucosa exhibit an activated profile and produce IL-17. Eur J Immunol **2019**; 49:133–43.
10. Gherardin NA, Souter MN, Koay HF, et al. Human blood MAIT cell subsets defined using MR1 tetramers. Immunol Cell Biol **2018**; 96:507–25.
11. Dias J, Boulouis C, Gorin JB, et al. The $CD4^{-}CD8^{-}$ MAIT cell subpopulation is a functionally distinct subset developmentally related to the main $CD8^{+}$ MAIT cell pool. Proc Natl Acad Sci U S A **2018**; 115:E11513–22.
12. Gibbs A, Leeansyah E, Introini A, et al. MAIT cells reside in the female genital mucosa and are biased towards IL-17 and IL-22 production in response to bacterial stimulation. Mucosal Immunol **2017**; 10:35–45.
13. Phetsouphanh C, Phalora P, Hackstein CP, et al. Human MAIT cells respond to and suppress HIV-1. Elife **2021**; 10:e50324.
14. Lukasik Z, Elewaut D, Venken K. MAIT cells come to the rescue in cancer immunotherapy? Cancers (Basel) **2020**; 12:413.
15. Healy K, Pavesi A, Parrot T, et al. Human MAIT cells endowed with HBV specificity are cytotoxic and migrate towards HBV-HCC while retaining antimicrobial functions. JHEP Rep **2021**; 3:100318.
16. Cosgrove C, Ussher JE, Rauch A, et al. Early and nonreversible decrease of $CD161^{++}$/MAIT cells in HIV infection. Blood **2013**; 121:951–61.

17. Leeansyah E, Ganesh A, Quigley MF, et al. Activation, exhaustion, and persistent decline of the antimicrobial MR1-restricted MAIT-cell population in chronic HIV-1 infection. Blood **2013**; 121:1124–35.
18. Lal KG, Kim D, Costanzo MC, et al. Dynamic MAIT cell response with progressively enhanced innateness during acute HIV-1 infection. Nat Commun **2020**; 11:272.
19. Leng T, Akther HD, Hackstein C-P, et al. TCR and inflammatory signals tune human MAIT cells to exert specific tissue repair and effector functions. Cell Rep **2019**; 28: 3077–91.e5.
20. Tincati C, Douek DC, Marchetti G. Gut barrier structure, mucosal immunity and intestinal microbiota in the pathogenesis and treatment of HIV infection. AIDS Res and Ther **2016**; 13:19.
21. Hirbod T, Kimani J, Tjernlund A, et al. Stable CD4 expression and local immune activation in the ectocervical mucosa of HIV-infected women. J Immunol **2013**; 191:3948–54.
22. Hasselrot K, Cheruiyot J, Kimani J, Ball TB, Kaul R, Hirbod T. Feasibility and safety of cervical biopsy sampling for mucosal immune studies in female sex workers from Nairobi, Kenya. PLoS One **2012**; 7:e47570.
23. Lajoie J, Boily-Larouche G, Doering K, et al. Improving adherence to post-cervical biopsy sexual abstinence in Kenyan female sex workers. Am J Reprod Immunol **2016**; 76:82–93.
24. Lajoie J, Tjernlund A, Omollo K, et al. Increased cervical $CD4^+CCR5^+$ T cells among Kenyan sex working women using depot medroxyprogesterone acetate. AIDS Res Hum Retroviruses **2019**; 35:236–46.
25. Juno JA, Boily-Larouche G, Lajoie J, et al. Collection, isolation, and flow cytometric analysis of human endocervical samples. J Vis Exp **2014**; 89:51906.
26. Tjernlund A, Carias AM, Andersson S, et al. Progesterone-based intrauterine device use is associated with a thinner apical layer of the human ectocervical epithelium and a lower ZO-1 mRNA expression. Biol Reprod **2015**; 92:68.
27. Buggert M, Frederiksen J, Noyan K, et al. Multiparametric bioinformatics distinguish the CD4/CD8 ratio as a suitable laboratory predictor of combined T cell pathogenesis in HIV infection. J Immunol **2014**; 192:2099–108.
28. Gibbs A, Hirbod T, Li Q, et al. Presence of $CD8^+$ T cells in the ectocervical mucosa correlates with genital viral shedding in HIV-infected women despite a low prevalence of HIV RNA-expressing cells in the tissue. J Immunol **2014**; 192:3947–57.
29. Livak KJ, Schmittgen TD. Analysis of relative gene expression data using real-time quantitative PCR and the $2^{-\Delta\Delta CT}$ method. Methods **2001**; 25:402–8.
30. Parrot T, Healy K, Boulouis C, et al. Expansion of donor-unrestricted MAIT cells with enhanced cytolytic function suitable for TCR redirection. JCI Insight **2021**; 6:e140074.
31. Healy K, Pavesi A, Parrot T, et al. Human MAIT cells endowed with HBV specificity are cytotoxic and migrate towards HBV-HCC while retaining antimicrobial functions. JHEP Rep **2021**; 3:100318.
32. Davanian H, Gaiser RA, Silfverberg M, et al. Mucosal-associated invariant T cells and oral microbiome in persistent apical periodontitis. Int J Oral Sci **2019**; 11:16.
33. Gibbs A, Sobkowiak MJ, Sandberg JK, Tjernlund A. In situ detection of MAIT cells and MR1-expressing cells in tissue biopsies utilizing immunohistochemistry. Methods Mol Biol **2020**; 2098:83–94.
34. Anahtar MN, Bowman BA, Kwon DS. Efficient nucleic acid extraction and 16S rRNA gene sequencing for bacterial community characterization. J Vis Exp **2016**; 110:53939.
35. Hamann D, Baars PA, Rep MH, et al. Phenotypic and functional separation of memory and effector human $CD8^+$ T cells. J Exp Med **1997**; 186:1407–18.
36. Godfrey DI, Koay HF, McCluskey J, Gherardin NA. The biology and functional importance of MAIT cells. Nat Immunol **2019**; 20:1110–28.
37. Juno JA, Phetsouphanh C, Klenerman P, Kent SJ. Perturbation of mucosal-associated invariant T cells and iNKT cells in HIV infection. Curr Opin HIV AIDS **2019**; 14:77–84.
38. Nel I, Bertrand L, Toubal A, Lehuen A. MAIT cells, guardians of skin and mucosa? Mucosal Immunol **2021**; 14:803–14.
39. Bister J, Crona Guterstam Y, Strunz B, et al. Human endometrial MAIT cells are transiently tissue resident and respond to *Neisseria gonorrhoeae*. Mucosal Immunol **2021**; 14:357–65.
40. Constantinides MG, Link VM, Tamoutounour S, et al. MAIT cells are imprinted by the microbiota in early life and promote tissue repair. Science **2019**; 366:eaax6624.
41. Merlini E, Cerrone M, van Wilgenburg B, et al. Association between impaired Vα7.2 + CD161++CD8+ (MAIT) and Vα7.2 + CD161-CD8+ T-cell populations and gut dysbiosis in chronically HIV- and/or HCV-infected patients. Front Microbiol **2019**; 10:1972.
42. Lepore M, Kalinichenko A, Colone A, et al. Parallel T-cell cloning and deep sequencing of human MAIT cells reveal stable oligoclonal TCRβ repertoire. Nat Commun **2014**; 5: 3866.